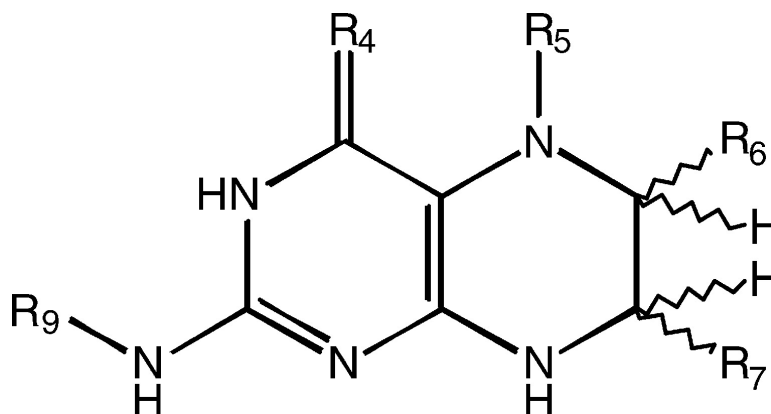Article

# Structural Analysis of Isoform-Specific Inhibitors Targeting the Tetrahydrobiopterin Binding Site of Human Nitric Oxide Synthases

Hans Matter, H. S. Arun Kumar, Roman Fedorov, Armin Frey, Peter Kotsonis,
Elisabeth Hartmann, Lothar G. Frhlich, Andreas Reif, Wolfgang Pfleiderer,
Peter Scheurer, Dipak K. Ghosh, Ilme Schlichting, and Harald H. H. W. Schmidt

## More About This Article

Additional resources and features associated with this article are available within the HTML version:

- Supporting Information
- Links to the 1 articles that cite this article, as of the time of this article download
- Access to high resolution figures
- Links to articles and content related to this article
- Copyright permission to reproduce figures and/or text from this article

**View the Full Text HTML**

# Structural Analysis of Isoform-Specific Inhibitors Targeting the Tetrahydrobiopterin Binding Site of Human Nitric Oxide Synthases

Hans Matter,[†] H. S. Arun Kumar,[*,‡] Roman Fedorov,[§,⊗] Armin Frey,[⊥] Peter Kotsonis,[⊥] Elisabeth Hartmann,[§] Lothar G. Fröhlich,[⊥] Andreas Reif,[⊥] Wolfgang Pfleiderer,[||] Peter Scheurer,[#] Dipak K. Ghosh,[▽] Ilme Schlichting,[§,⊗] and Harald H. H. W. Schmidt[⊥,‡,△]

*Sanofi-Aventis, Chemical Sciences, Drug Design, Building G 878, D-65926 Frankfurt am Main, Germany, Max Planck Institut für Molekulare Physiologie, Abt. Biophysikalische Chemie, Otto-Hahn-Strasse 11, D-44227 Dortmund, Germany, Institut für Pharmakologie und Toxikologie, Bayerische Julius-Maximilians-Universität Würzburg, Versbacher Strasse 9, D-97078 Würzburg, Germany, Fakultät für Chemie, Universität Konstanz, D-78434 Konstanz, Germany, Vasopharm BIOTECH GmbH, Winchester Strasse 2, D-35398 Giessen, Germany, Duke University and VA Medical Center, Durham, NC 27713, Max Planck Institut für Medizinische Forschung, Abt. Biomolekulare Mechanismen, Jahnstrasse 29, D-69120 Heidelberg, Germany, Rudolf-Buchheim-Institut für Pharmakologie, Justus-Liebig-Universität, Frankfurter Strasse 107, 35392 Giessen, Germany, Department of Pharmacology, Monash University, Melbourne, Victoria 3800, Australia*

Nitric oxide synthesized from L-arginine by nitric oxide synthase isoforms (NOS-I−III) is physiologically important but also can be deleterious when overproduced. Selective NOS inhibitors are of clinical interest, given their differing pathophysiological roles. Here we describe our approach to target the unique NOS (6*R*,1′*R*,2′*S*)-5,6,7,8-tetrahydrobiopterin (H₄Bip) binding site. By a combination of ligand- and structure-based design, the structure−activity relationship (SAR) for a focused set of 41 pteridine analogues on four scaffolds was developed, revealing selective NOS-I inhibitors. The X-ray crystal structure of rat NOS-I dimeric-oxygenase domain with H₄Bip and L-arginine was determined and used for human isoform homology modeling. All available NOS structural information was subjected to comparative analysis of favorable protein−ligand interactions using the GRID/concensus principal component analysis (CPCA) approach to identify the isoform-specific interaction site. Our interpretation, based on protein structures, is in good agreement with the ligand SAR and thus permits the rational design of next-generation inhibitors targeting the H₄Bip binding site with enhanced isoform selectivity for therapeutics in pathology with NO overproduction.

## Introduction

NO synthases (NOSs) are multidomain proteins consisting of a heme-containing catalytic oxygenase domain, a calmodulin-binding linker, and a NADPH reductase domain that catalyze the formation of NO from L-arginine, oxygen, and electrons.[1] The three isoforms of NOS are involved in several pathological processes, including Alzheimer's disease and stroke (NOS-I or nNOS), septic shock, arthritis, and inflammation (NOS-II or iNOS), and edema formation and reperfusion injury (NOS-III or eNOS).[1] Hence, the need for the discovery of isoform-selective NOS inhibitors is envisaged for specific therapeutic outcomes.[2]

All NOS isoforms are structurally similar with highly conserved active sites, as revealed by X-ray crystal structures.[3−9] Computational[10] and experimental studies[9,11] revealed differences at only one active site residue involved in the recognition of the L-arginine carbonyl oxygen (NOS-I Asp597 versus NOS-III Asn368),[12] which is a ligand motif in constrained peptidomimetic NOS-I inhibitors.[12−14] Consequently, most arginine-site directed inhibitors show only minimal isoform selectivity (except for a series of dipeptide amides and constrained peptidomimetics)[12−14] and long-term cross-reactivity with other heme-containing or arginine-binding enzymes cannot be ruled out a priori.

An alternative strategy arises from the fact that NOSs are the only heme-containing enzymes that require (6*R*,1′*R*,2′*S*)-5,6,7,8-tetrahydrobiopterin (H₄Bip) for maximal activation. The binding site within the oxygenase domain, differs structurally compared to other pterin-dependent enzymes such as aromatic amino acid hydroxylases[15] and, importantly, has noticeable amino acid differences among the NOS family. Since H₄Bip is essential for catalysis, dimer stabilization, or both, the H₄Bip binding site is a promising target for isoform-specificity and thus reduction of the side effects.

Many pteridine-based NOS inhibitors were previously shown to bind specifically and reversibly to the H₄Bip binding site.[15−20] In animal models of disease, these ligands were demonstrated to be beneficial. To mention a few, in allograft rejection, survival was prolonged with similar efficacy as high doses of cyclosporin A,[21] while in septic shock, 4-amino-H₄Bip is superior to the substrate-based inhibitor *N*^G-monomethyl-L-arginine in improving survival.[22] The analysis of structural prereq-

* Correspondence to Dr. H. S. Arun Kumar, D.B.A., D.V.M., Ph.D., Rudolf-Buchheim-Institute for Pharmacology, Frankfurter Str. 107, D-35392 Giessen, Germany. Tel: 0049 641 99-47631. Fax: 0049 641 99-47619. E-mail: Kumar.Arun@pharma.med.uni-giessen.de.
† Sanofi-Aventis.
‡ Justus-Liebig-Universität.
§ Max Planck Institut für Molekulare Physiologie.
⊥ Bayerische Julius-Maximilians-Universität Würzburg.
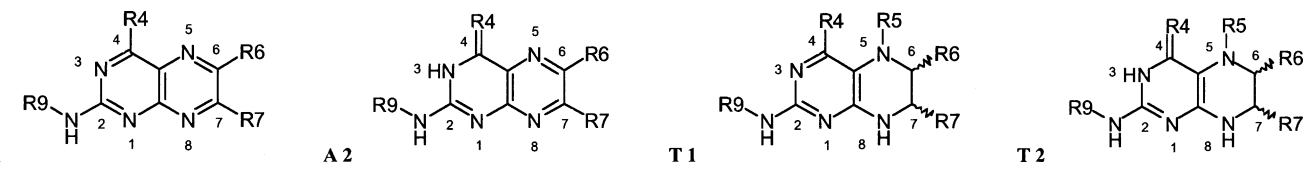|| Universität Konstanz.
# Vasopharm BIOTECH GmbH.
▽ Duke University and VA Medical Center.
⊗ Max Planck Institut für Medizinische Forschung.
△ Monash University.

**Table 1.** IC$_{50}$ Values of Selected Pteridine-Based NOS-I Inhibitors[a]



| | pteridine scaffold and substituents | | | | | | IC$_{50}$ ($\mu$M) | | | selectivity[b] | | |
| --- | --- | --- | --- | --- | --- | --- | --- | --- | --- | --- | --- | --- |
| PHS no. | scaffold | R4 | R5 | R6 | R7 | R9 | hNOS-I | hNOS-II | hNOS-III | II/I | III/I | III/II |
| 2 | A2 | O | | CH$_2$OCH$_2$-CH$_3$ | H | H | >500 | >500 | >500 | | | |
| 341 | A2 | O | | 1-naphthyl | H | H | 85.10 | >500 | 350.70 | >5.8 | 4.12 | <0.70 |
| 339 | A2 | O | | 4-FPh | H | H | 65.51 | >500 | 253.00 | >7.6 | 3.86 | <0.51 |
| 183 | A2 | O | | CH$_2$OCO-[4-(N=N)-(CF$_3$)CPh] | H | H | 33.46 | 374.20 | 208.60 | 11.18 | 6.23 | 0.56 |
| 303 | A1 | N(CH$_2$Ph)$_2$ | | Ph | H | H | 129.30 | 451.80 | 343.40 | 3.49 | 2.66 | 0.76 |
| 305 | A1 | N(CH$_2$Ph)$_2$ | | 4-CH$_3$OPh | H | H | 34.72 | 400.00 | 160.00 | 11.52 | 4.61 | 0.40 |
| 28 | T2 | O | H | CH$_2$NHCH$_3$ | H | H | 3.90 | 10.57 | 4.12 | 2.71 | 1.06 | 0.39 |
| 30 | T2 | O | H | CH$_2$OCO-[CH(NH$_2$)-(CH$_3$)] | H | H | 116.90 | >500 | >500 | >4.3 | >4.3 | <4.28 |
| 32 | T2 | O | COOCH$_2$-R6 | cyclic R5−R6 | H | H | 22.35 | 37.44 | 10.05 | 1.68 | 0.45 | 0.27 |
| 56 | T2 | O | COPh | H | H | H | >500 | >500 | >500 | | | |
| 72 | T2 | O | CO-3-pyridinium-1-CH$_2$Ph | Ph | Ph | COCH(CH$_3$)$_2$ | 111.10 | 122.70 | 253.20 | 1.10 | 2.28 | 2.06 |
| 331 | T1 | N(C$_3$H$_7$)$_2$ | H | Ph | H | H | 15.72 | 229.80 | 48.14 | 14.62 | 1.15 | 0.21 |
| 332 | T1 | N(C$_3$H$_7$)$_2$ | H | 4-CH$_3$OPh | H | H | 9.28 | 280.50 | 54.64 | 30.23 | 3.91 | 0.19 |
| 203 | T1 | NH$_2$ | H | CHOHCH-OHCH$_3$ | H | H | 1.26 | 1.70 | 5.46 | 1.35 | 4.33 | 3.21 |
| 330 | T1 | piperidino | H | 4-ClPh | H | H | 10.56 | 106.20 | 14.71 | 10.06 | 1.39 | 0.14 |
| 333 | T1 | N(C$_2$H$_5$)$_2$ | H | 4-ClPh | H | H | 13.97 | 307.40 | 56.66 | 22.01 | 4.06 | 0.18 |
| 334 | T1 | NH(CH$_2$-C$_6$H$_{11}$) | H | 4-ClPh | H | H | 3.68 | 214.20 | 31.71 | 58.20 | 8.62 | 0.15 |

[a] Incubation time was 30 min in the presence of 2 $\mu$M H$_4$Bip; Antipterins were used in the concentration range from 1 to 1000 $\mu$M (seven data points, all fits $r^2$ > 0.95). Control values were determined without antipterins. For experimental details, see Experimental Section. A denotes aromatic scaffold; T denotes tetrahydro scaffold; R represents substituents; Ph denotes phenyl. [b] Selectivity is defined as the ratio of the two IC$_{50}$ values (e.g., II/I represents (IC$_{50}$ for hNOS-II)/(IC$_{50}$ for hNOS-I), that is, the substance is *x*-fold more selective for hNOS-I over hNOS-II).

uisites for NOS inhibitor binding[23] prompted us to examine the determinants for isoform selectivity of this series with respect to other NOS isoforms.

We here apply two strategies to identify and validate selective inhibitors targeting NOS-I using ligand and protein structure-based approaches. First, the structure−activity relationship of a focused set of 41 pteridine analogues based on four different scaffolds was established for all three recombinant human NOS isozymes. Systematic variations at positions 4, 5, 6, and 7 of these chemotypes revealed substitutions with up to 58-fold selectivity for NOS-I compared to other isoforms in these assays.

To complement the identification of selective inhibitors and focus on structural reasons for selectivity, the X-ray crystal structure of the rat NOS-I oxygenase dimer, (unknown at the start of this project), was determined initially to a resolution of 2.0 Å with bound H$_4$Bip, then at 2.5 Å with bound H$_4$Bip and L-arginine substrate. Both experimental structures served to construct a homology model for the dimeric oxygenase domain of the human NOS-I isoform.[23]

Understanding the structural differences among NOS isoforms in the H$_4$Bip binding site is paramount in guiding rational design of selective inhibitors. Consequently the structural information derived from the human and mammalian NOS isoforms was subjected to chemometrical analysis of favorable protein−ligand interactions using the GRID/CPCA strategy.[24] This approach based on the GRID force field[25−29] highlights regions among all H$_4$Bip binding sites showing significant differences in their potential recognition of ligands. The method was also successfully applied for the NOS L-arginine binding site,[14] serine proteases,[24,31] cytochrome P450s,[32] kinases,[33] and matrix metalloproteinases.[34] In general, the computed binding site profiles derived from the GRID force field are analyzed using principal component analysis (PCA) to simplify the complex information, while consensus PCA (CPCA)[30] is a recent development to handle protein−ligand interactions from different field types (i.e., polar versus hydrophobic). The combined interpretation of the data from the focused ligand series, X-ray crystal structures, and comparative binding site analysis may be of value in guiding the design of the next-generation H$_4$Bip inhibitors with greater selectivity.

## Results and Discussion

**Structure−Activity Relationship of Selective Inhibitors.** Forty-one pteridine analogues were tested for isoform-selectivity against three human NOS isoforms (hNOS) using known assays.[15,35] Table 1 summarizes the biological data for the most active compounds. Previously we observed that varying 6- and

7-positions of the reduced antiperins with oxo (A2 or T2) or amino (A1 or T1) groups on position 4 of a tetrahydro (T) or aromatic (A) pteridine scaffold resulted in potent porcine NOS-I (pNOS) inhibitors.[19,23,36] This is confirmed for human NOS-I, where also substitution in positions 4, 5, 6, and 7 of aromatic and reduced pteridines was essential for affinity and selectivity. Importantly, bulky, hydrophobic substituents at R5 or R6 and alkylation of the 4-amino group with hydrophobic groups increased hNOS-I selectivity compared to hNOS-II or -III.

Replacing small groups at R6 by bulky, hydrophobic ones such as phenyl (PHS 341/339) or oxycarbonyl (PHS 183) resulted in antiperins with 30−100 $\mu$M $IC_{50}$ values and hNOS-I selectivity. In particular, PHS 183 was 11- and 6-fold selective for hNOS-I vs -II and -III.

Replacing the 4-oxo group by substituted amines led to aromatic 2,4-diaminopteridines (scaffold A1; PHS 303, 305). Binding affinity was increased by dibenzylation of the 4-amino group combined with phenyl (PHS 303) or 4-methoxyphenyl (PHS 305) at R6. Specific 4-amino modifications and favorable changes at position 6 led to the most selective inhibitors. PHS 305 has an $IC_{50}$ of 35 $\mu$M for hNOS-I and selectivity of 12 (hNOS-I/-II), whereas PHS 303 has an hNOS-I $IC_{50}$ of 129 $\mu$M and a selectivity of 3 (hNOS-I/-II/-III).

Favorable substitutions were identified for reduced 4-oxo pteridines (scaffold T2; PHS 28, 30, 32, 56, 72). PHS 28 with a methylaminomethyl group at R6 had an $IC_{50}$ value of 5 $\mu$M for all isoforms, while an acetyloxy substituent (PHS 30) at R6 is detrimental (PHS 30 $IC_{50}$ = 117 to >500 $\mu$M). Acylation at *N*-5 with benzoyl or benzoylnicotinoylium is also detrimental (PHS 72, $IC_{50}$ > 100 $\mu$M), but PHS 32 with a cyclic urethane is a moderate, nonselective inhibitor (hNOS-I $IC_{50}$ = 22 $\mu$M).

Finally, alkylated 4-amino-tetrahydropteridines (scaffold T1; PHS 331, 332, 203, 330, 333, 334) were potent and selective NOS inhibitors. Although PHS 203 is the best inhibitor ($IC_{50}$ = 1−5 $\mu$M for all isoforms), it lacks efficacy, while full enzyme inhibition (to 0% of $V_{max}$) was observed for 4-amino alkylated pteridines with hydrophobic, electron-rich phenyl (PHS 331), 4-methoxyphenyl (PHS 332), or 4-chlorophenyl (PHS 330, 333 and 334) substituents at R6 ($IC_{50}$ = 4−16 $\mu$M). These types of inhibitors were selective up to 58-fold for hNOS-I versus hNOS-II (PHS 334). In particular, the 4-methoxy substitution of the R6 phenyl ring influenced affinity (PHS 331 vs PHS 332; hNOS-I $IC_{50}$ = 16 vs 9 $\mu$M) and selectivity (hNOS-I/-II 15−30). Hence, steric bulk and physicochemical properties of alkyl groups attached to 4-amino pteridines with R6 *para*-chlorophenyl (PHS 330, PHS 333 and PHS 334) were crucial for affinity and isoform selectivity. Remarkably, one of the most potent and selective hNOS-I inhibitors was obtained by adding a hydrophobic cyclohexylmethyl group at the amine in R4 (PHS 334; hNOS-I $IC_{50}$ = 3.68 $\mu$M; selectivity hNOS-I/-II 58.2, hNOS-I/-III 8.6). Thus, bulky and hydrophobic substituents at R5 or R6 combined with appropriate alkylation of the 4-amino group preferably by hydrophobic substituents increased inhibition and selectivity to hNOS-I compared to NOS-II and -III, thus demonstrating the effect of hydrophobicity and steric bulk in these regions of the NOS-I $H_4Bip$ binding site.

**Table 2.** Data and Refinement Statistics of the Crystal Structure Determination of NOS-$I_{oxy}$

| | NOS-$I_{oxy}$ complexed with | |
| --- | --- | --- |
| | $H_4Bip$, no substrate | $H_4Bip$, L-arginine |
| PDB code | 1ZVI | 1ZVL |
| *Crystal Parameters* | | |
| space group | C222$_1$ | P2$_1$2$_1$2$_1$ |
| cell parameters: *a, b, c* (Å) | 43.2, 107.5, 163.0 | 52.4, 111.3, 165.2 |
| *Data Collection* | | |
| ESRF beamline | ID14-1 | ID14-2 |
| wavelength (Å) | 0.934 | 0.933 |
| resolution of data (Å) | 2.0 | 2.5 |
| no. of obsns/unique reflns[a] | 72678/24173 | 181445/32016 |
| completeness (total/high) %[a] | 92.3/79.5 | 93.4/79.6 |
| $\langle I/\sigma(I)\rangle$ (total/high)[a] | 11.0/4.4 | 14.3/4.5 |
| $R_{sym}$ (total/high) %[a,b] | 5.7/23.9 | 9.2/34.4 |
| *Refinement Statistics* | | |
| resolution range (Å) | 8.0−2.0 | 8.0−2.5 |
| included amino acids | 297−716 | 297−716 |
| no. of protein atoms | 3395 | 2 × 3419 |
| no. of waters | 150 | 324 |
| $R_{work}/R_{free}$ %[c] | 19.9/25.5 | 20.1/24.9 |
| rms deviation for bonds (Å)/angles (deg) | 0.008/1.2 | 0.009/1.3 |

[a] Completeness, $R_{sym}$, and $\langle I/\sigma(I)\rangle$ are given for all data and for the highest resolution shell. Substrate-free: 2.0−1.9 Å. L-Arg: 2.5−2.4 Å. [b] $R_{sym} = \Sigma|I - \langle I\rangle|/\Sigma I$. [c] $R_{work} = \Sigma|F_{obsd}| - k|F_{calcd}|/\Sigma|F_{obsd}|$; 5% of randomly chosen reflections were used for the calculation of $R_{free}$.

**Crystal Structures of Rat NOS-I Oxygenase Domains.** To understand the structural basis for NOS isoform specificity by pteridine analogues, the ligand SAR is complemented with a comparative analysis of different NOS binding sites. Structural information for NOS-I was not available at the start of the project; we determined the crystal structure of oxygenase domain of rat NOS-I in the presence/absence of substrate L-arginine (Table 2). As expected, the overall structure corresponds to those of NOS-II and -III with the $H_4Bip$ binding site topology (Figure 1) being very similar to rat NOS-I oxygenase dimer.[8,9,12,14] The main interactions in the rat NOS-I $H_4Bip$ binding site linked to binding affinity indicated differences in hydrogen bond interactions, distances between heavy atoms (Å), and amino acid sequence compared to those in NOS-I and -III (Figure 2). Finally, differences within a radius of 8 Å around $H_4Bip$ in its experimental position are indicated.

The cofactor $H_4Bip$ is deeply buried in the cavity and not accessible to bulk solvent, it is oriented proximal and perpendicular to heme. The main protein−ligand interaction as in other pterin−protein complexes, occurs between the planar $H_4Bip$ ring and the Trp678 indole, stacked at 3.6 Å distance.[37,38] In general, the hydrogen-bond pattern corresponds to $H_4Bip$ bound to NOS-II or -III.[3−5] The 5,6,7,8-tetrahydropteridine interacts with heme carboxylate (O4 via solvent, N3 directly); the structurally conserved water is present in related X-ray structures. The C4-carbonyl oxygen is hydrogen-bonded to Arg596 guanidine from the substrate binding helix. For the NOS-II monomer, this part is disordered, explaining that only dimeric NOS with properly oriented Arg596 binds $H_4Bip$. The entrance to the $H_4Bip$ binding region is occupied by Met336 and Leu337 side chains, the latter is present in rat NOS-I but replaced by
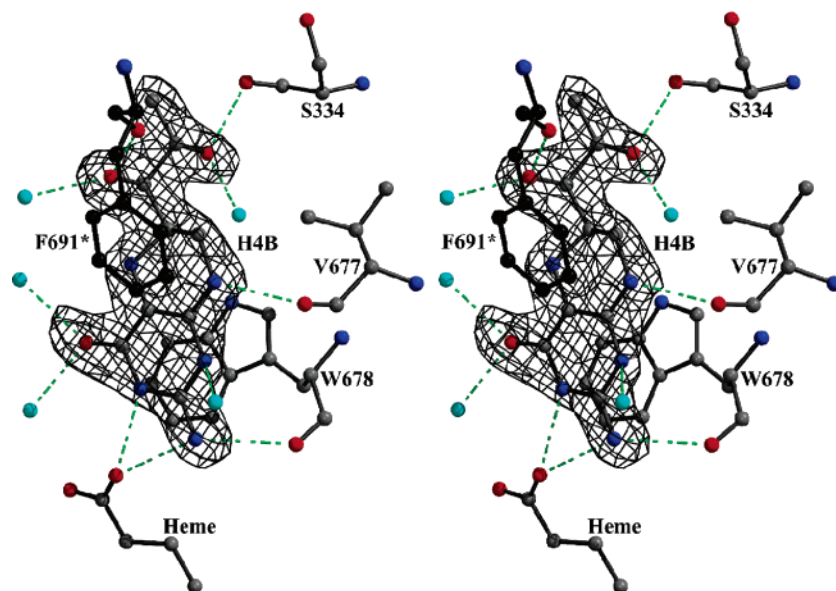
**Figure 1.** Stereoview of $F_{obsd} - F_{calcd}$ difference electron density map contoured at $3\sigma$ showing the H$_4$Bip binding site in the oxygenase domain of rat NOS-I. Hydrogen bonds are indicated by dotted lines and water molecules by cyan spheres; atoms are colored by elements: carbon, gray; oxygen, red; nitrogen, blue. F691, marked by an asterisk, belongs to the other molecule in the biological dimer.
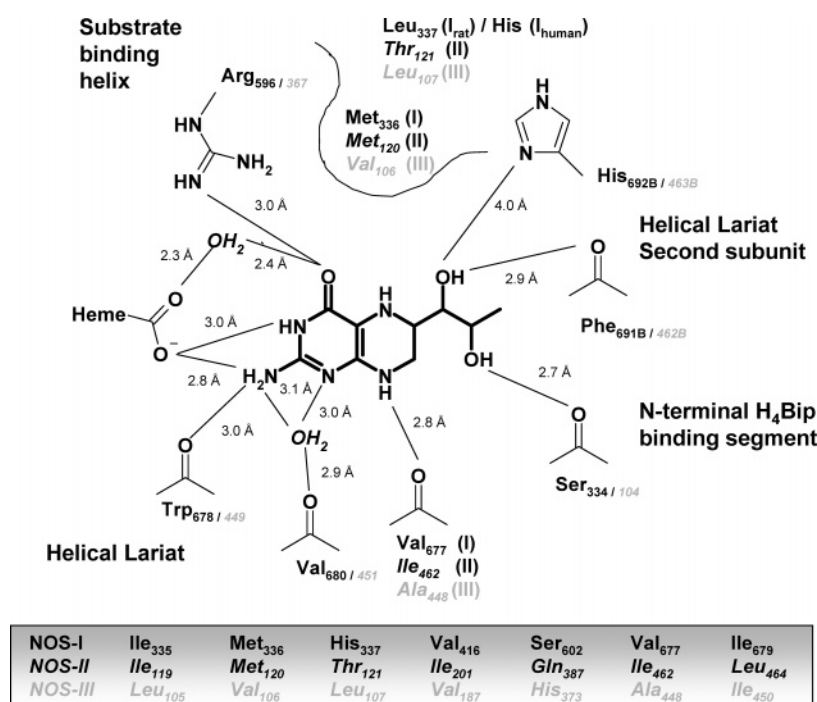


**Figure 2.** Schematic of the interaction of H$_4$Bip in the rat NOS-I binding site and the amino acid differences among all three NOS isoforms. The rat NOS-I residue numbering is given in black with NOS-III numbering (grey) in comparison.

histidine in the human NOS-I ortholog. These 2-amino-groups interact with the heme carboxylate and the backbone carbonyl group of Trp678. Finally N8 is in close hydrogen bonding with the carbonyl group of Val677, which is replaced by Ala448 in NOS-III. The H$_4$Bip dihydroxypropyl side chain occupies a pocket formed by side chains of Met336 (Val106 in NOS-III), TrpB676, TrpB306, and other backbone amide bonds. This polar chain interacts with Ser334 and PheB691 carbonyl oxygens and with HisB692 via structural water, present in other structures but not this X-ray structure.

**Docking and Homology Modeling.** To address our objective to design therapeutically useful hNOS-I inhibitors, we employed the rat NOS-I oxygenase X-ray structure to derive a homology model for the human ortholog. This model was generated using the program Composer[39−41] in analogy to a previous model.[23] Despite high sequence identity, there are changes close to the H$_4$Bip binding site, in particular the Leu337 versus His mutation in hNOS-I. This model and the rat NOS-I structure were used for docking studies. Figure 3 shows the binding mode for PHS 334 using QXP[42] in comparison to the experimental binding mode of H$_4$Bip in the
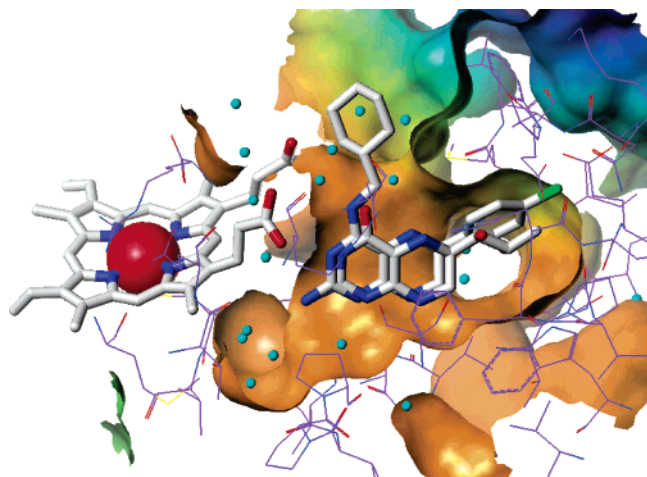
**Figure 3.** Comparison of the experimental H₄Bip binding mode in rat NOS-I and the best docking mode for PHS 334. Water molecules from the X-ray structure are indicated by cyan spheres; hydrogens are omitted for clarity. The NOS-I binding site is indicated by its solvent-accessible surface, color coded by cavity depth.

rat NOS-I X-ray structure. Hydrogens are omitted for clarity; the protein binding pocket is indicated using a solvent-accessible surface[43,44] colored by cavity depth.[45,46] Since the Monte Carlo based docking could reproduce H₄Bip orientation only with structural water molecules, these were further included. The postulated binding mode of PHS 334 is similar in both human and rat NOS-I cavities and agrees with that of H₄Bip with direct and potentially water-mediated interactions to heme propionic acid side chain. The 2-amino group is hydrogen bonded to heme and Trp678 C=O, while N1 interacts with the same residue via water. Replacing the C4 carbonyl oxygen by NH results in rearrangement of Arg596 or additional interaction involving water. The NH in position 8 is hydrogen bonded to Val677 C=O. The *p*-chlorophenyl substituent at C6 is directed toward a more hydrophobic pocket. This pocket, formed by side chains of Met336, Trp306B, Trp676B, and Glu694 and some backbone amide groups, accommodates the hydrophobic substituent. The side chain of Met336 plays a key role by interacting with the cyclohexylmethyl substituent at N4, thus contacting and stabilizing two hydrophobic groups in different subpockets. Replacement by the smaller Val106 in NOS-III resulted in less favorable interactions, which might partially explain the selectivity difference.

**Chemometrical Analysis of Selectivity Differences.** To investigate isoform-specific binding site interactions in NOS, we applied the GRID/CPCA strategy[24−28,33] to the rat and human NOS-I oxygenase structures described above and to 11 representative structures of other isoforms deposited in the PDB at the time of this study (Table 3). Favorable protein−ligand interactions were analyzed by PCA to understand similarities in protein binding sites. In addition to showing how different two binding sites are from the perspective of a ligand, PCA also unveils structural reasons for the discrimination. Different models were generated, while we will discuss the model using three GRID probes and a cutout region of 4 Å around PHS 334. This dataset served to derive submodels for pockets

**Table 3.** Protein Structures Used for NOS Target Family GRID/CPCA Analysis[a]

| structure | organism | method | resolution (Å) | ligand |
|-----------|----------|--------|----------------|--------|
| | | NOS-I (nNOS) | | |
| nnox | rat | X-ray | 2.0 | H₄Bip |
| nno2 | human | homology[b] | | |
| | | NOS-II (iNOS) | | |
| 1nsi | human | X-ray | 2.50 | H₄Bip |
| 2nsi | human | X-ray | 3.00 | H₄Bip |
| 4nos | human[c] | X-ray | 2.20 | H₄Bip |
| | | NOS-III (eNOS) | | |
| 1d1v | bovine | X-ray | 1.90 | H₄Bip |
| 1dmi | bovine | X-ray | 2.00 | H₄Bip |
| 1dmj | bovine | X-ray | 2.30 | 5,6-cyclic tetrahydro-pteridine PHS 32 |
| 1dmk | bovine | X-ray | 1.90 | 4-amino-6-phenyl-tetrahydropteridine |
| 1fop | bovine | X-ray | 2.30 | H₄Bip |
| 1nse | bovine | X-ray | 1.90 | H₄Bip |
| 2nse | bovine | X-ray | 2.30 | H₄Bip |
| 3nos | human | X-ray | 2.40 | H₄Bip |

[a] All proteins except nno2 and nnox were retrieved from Research Collaboratory for Structural Bioinformatics (RCSB). Ligands, metals, and counterions were removed except for heme next to the H₄Bip binding site. See RCSB entries for references. Dimers were constructed using the matrix given in the PDB header. [b] Built in according to ref 23 using nnox as templates. This model is based on the Genbank accession code P29475 after truncations of the N- and C- terminal parts. [c] Different N- and C-terminal truncations plus one mutation compared to 1nsi and 2nsi.
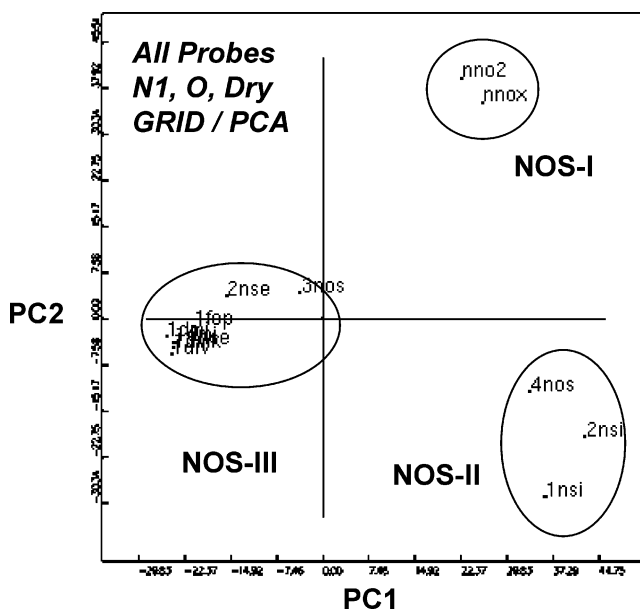


**Figure 4.** Score plot for the GRID/PCA analysis with three NOS isoforms and a 4 Å region around PHS 334. The clustering of binding sites in these score plots results only from similar protein−ligand 3D interaction patterns and not from 1D sequence similarity.

filled with PHS 334 cyclohexyl and *p*-chlorophenyl substituents, respectively.

The PCA score plot for the NOS family is shown in Figure 4. The first principle component (*x*-axis in Figure 4) reveals separation of NOS-I and -II on the right (positive PC1 scores) from NOS-III, including human (3nos) and bovine isotypes. The second component (*y*-axis) separates NOS-I (positive PC2 scores) from other isoforms. The contributions of amide nitrogen,
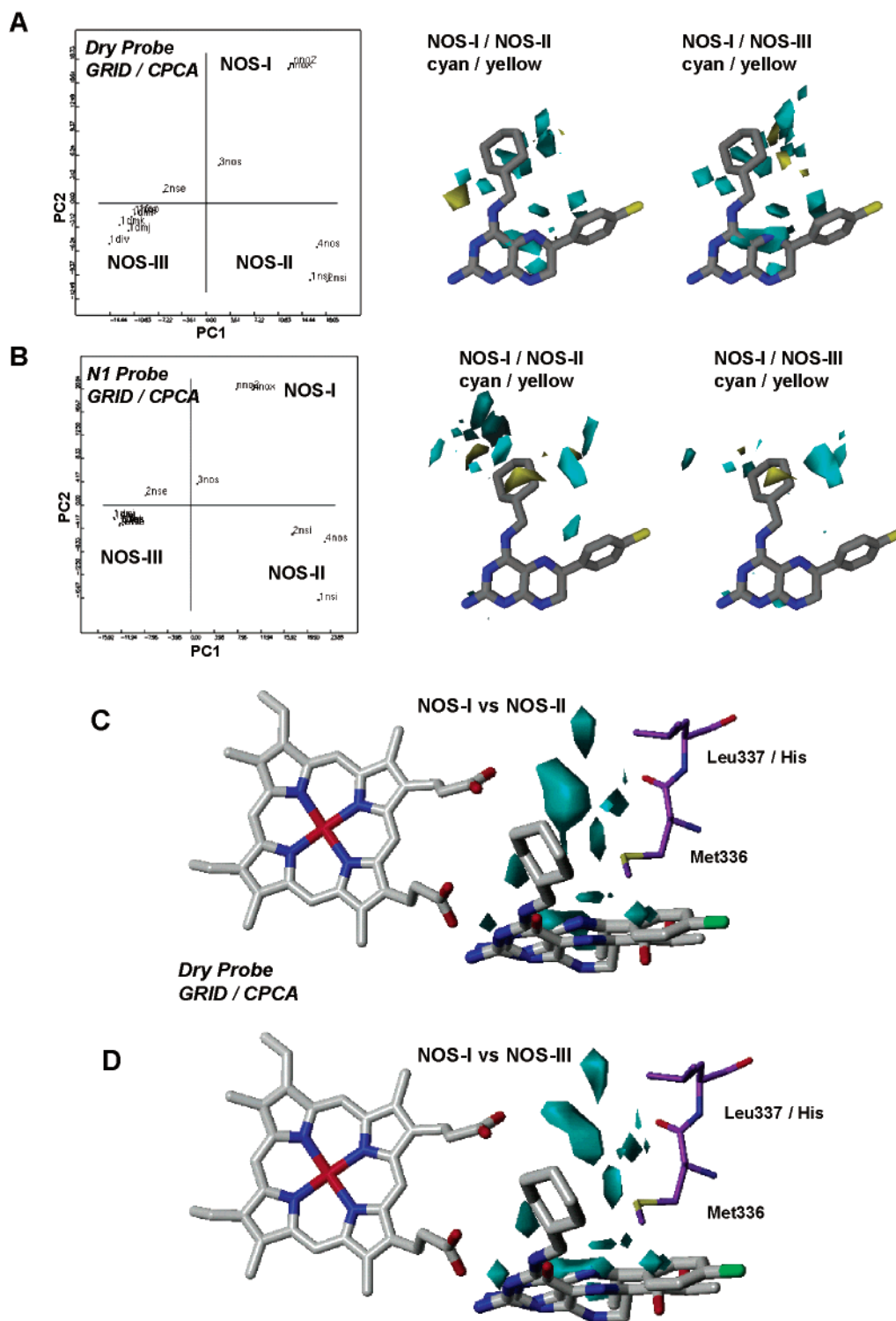
**Figure 5.** Score and GRID/CPCA differential plots. Panel A presents **a** focus on a 4 Å region around the cyclohexyl group in PHS 334 showing differences between NOS-I and NOS-II (middle) and NOS-I and NOS-III (right). Favorable GRID dry probe interactions for NOS-I selectivity are shown in cyan; unfavorable interactions are shown in yellow with respect to the PHS 334 docking mode. Panel B shows the same data as panel A for GRID amide N1 probe. Panel C shows GRID/CPCA differential plots for the dry probe mapped onto the rat NOS-I H4Bip binding site and PHS 334 and NOS-I key residues for selectivity close to the cyclohexyl substituent. Favorable interactions to achieve NOS-I isoform selectivity compared to NOS-II are indicated in cyan. Panel D shows the same data as panel C for NOS-I versus NOS-III selectivity.

carbonyl oxygen, and hydrophobic probes to the classification are similar and the corresponding picture for the NOS target family results in more GRID probes for this analysis.

The binding site interactions responsible for this discrimination in the cyclohexyl substituent pocket are highlighted in CPCA differential plots for amide nitrogen and hydrophobic GRID probes, and favorable interactions to only one NOS isoform for a 4 Å region around the PHS 334 cyclohexyl group are summarized (Figure 5). The CPCA score plots indicate clear separation between all NOS isoforms considering only interac-

tions in this pocket and the N1 or dry probes, respectively. Differences between NOS-I and -II and NOS-I and -III were visualized using PHS 334 as reference. Favorable and unfavorable GRID dry (Figure 5A) and amide nitrogen N1 (Figure 5B) interactions for NOS-I selectivity are shown in cyan and yellow, respectively. The favorable contours for NOS-I are mapped in Figure 5C,D onto the rat NOS-I $H_4Bip$ binding site with key NOS-I residues for selectivity close to the cyclohexyl substituent.

Contour regions indicating favorable interactions of ligand with NOS-I are located close to the PHS 334 cyclohexyl side chain, which is the major ligand motif for isoform selectivity (Table 1). Consistently, N1 and hydrophobic interactions provide the highest opportunity for isoform selectivity. Hydrophobic 4-amino substituents such as cyclohexylmethyl or piperidine positively influence NOS-I isoform selectivity (Figure 5A). The main amino acid differences in the binding pocket are Ile335/Ile/Leu (NOS-I/II/III), Met336/Met/Val, His337/Thr/Leu (Phe in human NOS-III, Leu in rat NOS-I) (Figures 2 and 5C,D). A hydrophobic substituent interacts more favorably with the larger Met337 (NOS-I) side chain and its surrounding Ile335 and His337/Leu compared to the shorter and more rigid valine in NOS-III, which correlates with ligand selectivity. Other mutations also influence discrimination among isoforms, especially Val677 against Ile or Ala (NOS-II/III). Favorable interactions are increased by hydrophobic substitutions of H4Bip dihydroxyisopropyl side chain. Cyan contours (Figure 5A) close to C7 at the central scaffold indicate favorable interactions to Val677 in NOS-I. This mutation influences selective interaction in the chlorophenyl substituent pocket, and substituents with increased hydrophobicity increased selectivity due to improved interactions to Val677 at its bottom and Met336–Leu/His337 at its upper edge. This is exemplified by cyan contours at the *p*-chlorophenyl substituent in PHS 334 (Figure 5A).

The interpretation of this study in terms of protein–ligand interactions for isoform discrimination is concurrent to the structure–activity relationship from the ligand binding data. Preference for hydrophobic interactions in both subpockets related to the PHS 334 chlorophenyl and cyclohexyl substituent from the GRID/CPCA study corresponds to the observation that bulky, more hydrophobic substituents at positions R5 or R6 of the presented scaffolds and alkylation of the 4-amino group using a hydrophobic substituent significantly improve selective inhibition of human NOS-I.

## Conclusions

This study describes our approach to target the unique NOS (6R,1′R,2′S)-5,6,7,8-tetrahydrobiopterin (H4Bip) binding site to identify selective inhibitors against the NOS-I isoform (neuronal NOS) based on a combination of ligand- and structure-based design. To this end, we determined the crystal structure of the dimeric oxygenase domain of the rat NOS-I isoform and employed it for building a homology model of the human isoform. Significant differences within H4Bip binding sites of different NOS isoforms were uncovered using ligand-based SAR and protein-based comparative binding site analysis using the GRID/CPCA approach. While

the latter analysis provided a meaningful classification of NOS structures by three-dimensional interaction patterns from the protein perspective, its interpretation in structural terms is in good agreement with the view of the ligands provided by SAR data. It was consistently found that hydrophobic substitutions at the N4 and C6 positions result in better affinity and enhanced selectivity for pteridine-based inhibitors. Antipterins with the tetrahydro scaffold are more active and selective than those with an aromatic one. The most selective NOS-I inhibitor targeting this binding site shows up to 58-fold selectivity for NOS-I compared to NOS-III, while significant improvements are to be expected. The structural knowledge of all NOS isoforms and the consistent interpretation of ligand- and structure-based approaches to extract protein family motifs linked to selective interaction to only one member allow for the next-generation rational design of inhibitors targeting this H4Bip binding site. The combined interpretation of the data from the focused ligand series, X-ray crystal structures, and comparative binding site analysis establish this site as a validated target for isoform-selective NOS inhibition and provide guidance for the design of next-generation H4Bip inhibitors with different (NOS-II/III) and greater NOS-I selectivity.

## Experimental Section

**Synthesis of Antipterins.** Pteridine derivatives were synthesized as described previously.[15,19,23,36]

**Purification of Human NOS.** Recombinant hNOS-I, -II, and -III were expressed in the baculovirus/Sf9 cell system and purified using sequential 2′,5′-ADP–Sepharose and CaM–Sepharose affinity chromatography steps (the latter step can only be applied with hNOS-I and -III), as previously described.[47,48]

**NOS Activity Assay.** NOS activity was measured by conversion of L-arginine to L-citrulline as previously described.[48] H4Bip at a final concentration of 2 $\mu$M, pteridines, or both were added as indicated. The standard assay time was 30 min, which was within the linear phase of product formation. The assay time for determination of basal activity and $K_{0.5}$ of H4Bip was 10 min. Some experiments were performed in the presence of catalase (500 U, 45 min).

**Enzyme Kinetic and Data Analysis.** The screening methodology and data analysis used here were similar to our previous work.[15,19,36] All concentration–response curves were characteristically sigmoidal (Prism software; GraphPad) employing the "built-in" fitting equation

$$\text{specific activity} = V_{\min} + \frac{V_{\max} - V_{\min}}{1 + 10^{(\log_{10}(EC_{50}) - \log_{10}(c))h}}$$

**Cloning, Purification, and Crystallization of Rat NOS-I Oxygenase Domain.** The rat nNOS oxygenase domain catalytic core unit (amino acids 291–722) was prepared using rat NOS-I cDNA as a template using a previously described procedure for generation of mouse and human NOS-II oxygenase domains.[49,50] The pCWori vector expressing nNOS was transformed into the proteinase-deficient *Escherichia coli* strain BL21DE3 (Novagen) and grown in the presence of 0.4 mM of the heme precursor $\delta$-aminolevulinic acid and 0.5 mM isopropyl $\beta$-D-thiogalactoside. The NOS-I oxygenase domain was purified using Ni²⁺ affinity and S75 gel filtration chromatography. The Δ290 NOS-I oxygenase domain retains characteristics of the native NOS-I oxygenase domain (amino acids 1–722). Crystals were grown in the dark at 20 °C by vapor diffusion using the hanging drop geometry. One microliter of protein solution (15 mg/mL in 40 mM EPPS, pH 7.6, 150 mM NaCl, 5% glycerol, 4 $\mu$M H4Bip, 2 mM $\beta$-mercapto-

ethanol, in the presence or absence of 10 mM L-arginine) and reservoir solutions (100 mM *N*-2-hydroxyethylpiperazine-*N'*-2-ethanesulfonic acid (Hepes), pH 7.0, 5 mM dithioerythritol (DTE), 130 mM $Ca^{2+}$-acetate, 30 mM spermine, and 20% (w/v) poly(ethylene glycol) (PEG) 3350) were mixed. Prior to flash cooling, crystals were rinsed in a cryoprotection solution consisting of the reservoir solution supplemented with 11.5% PEG 10 000.

**Diffraction Data Collection and Refinement.** Diffraction data were collected at 100 K at the ESRF using an ADSC CCD detector and reduced with the XDS program package[51] (cf. Table 2). The structure of the L-arginine-free NOS-I oxygenase domain was solved by molecular replacement using the coordinates of the bovine NOS-III oxygenase domain as a search model (PDB code 1d1w). Refinement was done with CNS[52] and included simulated annealing and individual *B*-factor refinement. During several cyclic rounds of refinement and manual rebuilding, a zinc ion, solvent molecules, and ligands were included in the models, which displayed good stereochemistry (Table 2).

**Homology Modeling and Docking.** A homology model for human NOS-I was generated using Composer[39−41] from rat NOS-I structures. A multiple alignment was generated across all sequences and assigned weights proportional to the square of their percentage sequence identity of the model sequence. 3D structural analysis using seed residue was performed, which lead to determination of structurally conserved regions (SCR). The unknown sequence (Genbank accession number P29475) was aligned to determine the location of SCR in the target sequence. A fragment from one of the homologues was used to model the backbone of each SCR, while a rule-based procedure was employed to model side chains. Structurally variable regions were constructed by selecting a fragment to model each loop region either from the corresponding location in a homologous protein or from the entire protein database. The NOS-I monomer was checked for steric overlap, superimposed onto other isoforms, and completed by adding heme, $H_4Bip$, and the second NOS-I monomer.

For docking using QXP,[42] only protein residues, heme, and selected structurally conserved water molecules within an 8 Å sphere around $H_4Bip$ were considered. Selected parts of the cavity were allowed to move during conformational searching. Conformers were ranked using estimated QXP total association energy[42] based on a modified AMBER force field.[53]

**GRID/CPCA Analysis.** Eleven structures of dimeric human NOS-II and human and bovine NOS-III with intact $H_4$-Bip binding sites were retrieved from the PDB (Table 3). For NOS-I, we used the crystal structure with $H_4Bip$ described here plus the homology model built for human brain NOS-I (Genbank accession number P29475). For all proteins, water, counterions, additional ligands, and heme cofactors not close to the $H_4Bip$ binding site were removed prior to computing GRID binding site profiles.

For binding site alignment, a multiple sequence alignment of all proteins was generated using Composer.[39−41] The seed residues served as a basis for 3D structural alignment, leading to the identification of structurally conserved regions (SCRs) among the entire protein ensemble. The X-ray structure of NOS-III (PDB 1nse) was used as reference. The SCRs were used for a pairwise rms fitting of corresponding backbone atoms of all proteins to the reference structure. In two iterations, amino acid pairs with a deviation larger than $3 \times$ SD from the previous solution were rejected, leading to an unambiguous alignment with an acceptable superposition of important structural elements.

A multivariate description of $H_4Bip$ binding sites for NOS oxygenase domains was done using the GRID force field[25−29] and three probes: an $sp^2$ carbonyl oxygen (O), a hydrophobic probe (DRY), and a neutral, flat amide probe (N1). All protein−ligand interactions were identified using a 1 Å grid spacing and static protein treatment (GRID directive MOVE = 0). Hydrogens were added to the aligned protein structures using the program GRIN. The GRID box dimensions were selected to include all relevant parts of the $H_4Bip$ binding sites.

The GRID molecular interaction field data were organized as previously described.[33] A vector is constructed for the interaction field of one probe and one protein. The interaction fields for other probes are concatenated to this vector to produce a long vector containing $x$ GRID $\times$ $n$ probe points. Similar vectors were derived for all proteins. At the end, the resulting X-matrix for analysis has one single row for each NOS 3D structures and $x \times n$ columns (i.e., GRID interaction points).

This X-matrix was analyzed using PCA and consensus PCA,[24] as implemented in GOLPE.[54,55] A maximum cutoff value of 0 kcal/mol was used to focus on favorable interaction energies and remove information related to steric repulsion. PCA studies including repulsive interactions do not qualitatively change the classifications. In addition, only GRID points within a radius of 4.0 Å around the ligand PHS 334 in its docked conformation were considered using the GOLPE region cutout tool for variable selection. Furthermore 2- and 3-level variables and columns with a SD below 0.02 as threshold were rejected. The data organization allows one to apply block unscaled weights scaling to normalize the importance of probe interactions in the final models. This method scales each a single probe−protein interaction field separately, whereas relative scales of variables within each block remain unchanged.

In PCA, the scaled data matrix X with interaction energies $x_{ik}$ for $i$ protein interactions and $k$ grid points is decomposed to means ($x_k$), scores ($t_{ia}$), loadings ($p_{ak}$), and residuals ($e_{ik}$), $a$ denoting the number of model dimensions:

$$x_{ik} = x_k + \sum_{a=1}^{A} t_{ia} p_{ak} + e_{ik}$$

The data matrix X is approximated by the product of two smaller matrices, scores, and loadings. The score matrix $p_{ak}$ gives a simplified picture of the objects (proteins interacting by multiple probes), represented by new uncorrelated variables. Scores plots can be used to visualize the grouping of NOS isoforms based on their protein−probe interaction pattern. The PCA of such an X matrix produces a scores plot where each protein structure is represented by a single point. Proteins with similar binding sites−especially those with a similar interaction pattern to adequate GRID probes−should then be clustered. The analysis then is able to focus on differences between individual isoforms. The first new principal component (PC) describes the maximum variance among all possible directions, the second one the next largest variation among all directions orthogonal to the first one, etc. The resulting eigenvalues represent the overall variance after extraction of each successive new factor. If most of the variation of the original data can be described by the first few factors, a much simpler data structure exists.

Consensus PCA (CPCA)[24] evaluates the relative importance of individual probes for the PCA model. Since the X data matrix is structured in meaningful blocks from GRID probe interaction fields, hierarchical PCA methods such as CPCA provide interesting information regarding the relative importance of the different blocks (i.e., probes) in the analysis. CPCA uses the same objective function as PCA to explain X-matrix variance. The analysis is made on a block level (i.e., individual probe-derived fields) and on a consensus level combining all blocks; the latter analysis is similar to a regular PCA. For each block, individual scores and loadings are obtained together with their relative importance for the consensus block. Block scores represent a particular, constrained submodel for a particular probe (i.e., interaction type) and add information that is not available from PCA. Those individual scores are plotted for analysis of the selectivity model for the remaining individual N1, O, and DRY probes. Block scores represent a particular point of view of the model given by a certain probe and provide unique information not present in regular the PCA model. Object distances in the block scores are used in GOLPE to assess the relative importance of the different probes in their discrimination.

The analysis of PCA and CPCA loadings plot containing information about the interaction fields between a GRID probe and the target protein structure is done using *active plots* in GOLPE plot options. Those active plots help to focus on those PCA or CPCA loadings that discriminate between NOS isoforms. They represent isocontour plots of GRID interaction field variables, which contribute most to explain differences between two manually specified objects in a scores plot of a PCA or CPCA model. Hence, these active plots greatly simplify the analysis step to result in a meaning chemical interpretation of selectivity differences. Based on a CPCA model, those plots can be obtained for each individual probe interaction field and thus answers the question which particular probe is responsible for an observed selectivity difference.

**Statistics.** The results shown represent mean values $\pm$ SEM. For comparisons, we used one- or two-way analysis of variance (ANOVA) followed by Dunnett's or Bonferroni's Multiple Comparison Test. A $P$ value of $<0.05$ was considered significant.

## References

(1) Alderton, W. K.; Cooper, C. E.; Knowles, R. G. Nitric oxide synthases: structure, function and inhibition. *Biochem. J.* **2001**, *357*, 593−615.

(2) Babu, B. R.; Griffith, O. W. Design of isoform-selective inhibitors of nitric oxide synthase. *Curr. Opin. Chem. Biol.* **1998**, *2*, 491−500.

(3) Crane, B. R.; Arvai, A. S.; Gachhui, R.; Wu, C.; Ghosh, D. K.; et al. The structure of nitric oxide synthase oxygenase domain and inhibitor complexes. *Science* **1997**, *278*, 425−431.

(4) Crane, B. R.; Arvai, A. S.; Ghosh, D. K.; Wu, C.; Getzoff, E. D.; et al. Structure of nitric oxide synthase oxygenase dimer with pterin and substrate. *Science* **1998**, *279*, 2121−2126.

(5) Raman, C. S.; Li, H.; Martasek, P.; Kral, V.; Masters, B. S.; et al. Crystal structure of constitutive endothelial nitric oxide synthase: a paradigm for pterin function involving a novel metal center. *Cell* **1998**, *95*, 939−950.

(6) Fischmann, T. O.; Hruza, A.; Niu, X. D.; Fossetta, J. D.; Lunn, C. A.; et al. Structural characterization of nitric oxide synthase isoforms reveals striking active-site conservation. *Nat. Struct. Biol.* **1999**, *6*, 233−242.

(7) Raman, C. S.; Li, H.; Martasek, P.; Babu, B. R.; Griffith, O. W.; et al. Implications for isoform-selective inhibitor design derived from the binding mode of bulky isothioureas to the heme domain of endothelial nitric-oxide synthase. *J. Biol. Chem.* **2001**, *276*, 26486−26491.

(8) Li, H.; Shimizu, H.; Flinspach, M.; Jamal, J.; Yang, W.; et al. The novel binding mode of *N*-alkyl-*N*′-hydroxyguanidine to neuronal nitric oxide synthase provides mechanistic insights into NO biosynthesis. *Biochemistry* **2002**, *41*, 13868−13875.

(9) Fedorov, R.; Hartmann, E.; Ghosh, D. K.; Schlichting, I. Structural basis for the specificity of the nitric-oxide synthase inhibitors W1400 and N(omega)-propyl-L-Arg for the inducible and neuronal isoforms. *J. Biol. Chem.* **2003**, *278*, 45818−45825.

(10) Ji, H.; Li, H.; Flinspach, M.; Poulos, T. L.; Silverman, R. B. Computer modeling of selective regions in the active site of nitric oxide synthases: implication for the design of isoform-selective inhibitors. *J. Med. Chem.* **2003**, *46*, 5700−5711.

(11) Flinspach, M. L.; Li, H.; Jamal, J.; Yang, W.; Huang, H.; et al. Structural basis for dipeptide amide isoform-selective inhibition of neuronal nitric oxide synthase. *Nat. Struct. Mol. Biol.* **2004**, *11*, 54−59.

(12) Gomez-Vidal, J. A.; Martasek, P.; Roman, L. J.; Silverman, R. B. Potent and selective conformationally restricted neuronal nitric oxide synthase inhibitors. *J. Med. Chem.* **2004**, *47*, 703−710.

(13) Hah, J. M.; Roman, L. J.; Martasek, P.; Silverman, R. B. Reduced amide bond peptidomimetics. (4*S*)-*N*-(4-amino-5-[aminoakyl]-aminopentyl)-*N*′-nitroguanidines, potent and highly selective inhibitors of neuronal nitric oxide synthase. *J. Med. Chem.* **2001**, *44*, 2667−2670.

(14) Hah, J. M.; Martasek, P.; Roman, L. J.; Silverman, R. B. Aromatic reduced amide bond peptidomimetics as selective inhibitors of neuronal nitric oxide synthase. *J. Med. Chem.* **2003**, *46*, 1661−1669.

(15) Bommel, H. M.; Reif, A.; Frohlich, L. G.; Frey, A.; Hofmann, H.; et al. Anti-pterins as tools to characterize the function of tetrahydrobiopterin in NO synthase. *J. Biol. Chem.* **1998**, *273*, 33142−33149.

(16) Werner, E. R.; Pitters, E.; Schmidt, K.; Wachter, H.; Werner-Felmayer, G.; et al. Identification of the 4-amino analogue of tetrahydrobiopterin as a dihydropteridine reductase inhibitor and a potent pteridine antagonist of rat neuronal nitric oxide synthase. *Biochem. J.* **1996**, *320*, 193−196.

(17) Reif, A.; Frohlich, L. G.; Kotsonis, P.; Frey, A.; Bommel, H. M.; et al. Tetrahydrobiopterin inhibits monomerization and is consumed during catalysis in neuronal NO synthase. *J. Biol. Chem.* **1999**, *274*, 24921−24929.

(18) Crane, B. R.; Arvai, A. S.; Ghosh, S.; Getzoff, E. D.; Stuehr, D. J.; et al. Structures of the $N^{\omega}$-hydroxy-L-arginine complex of inducible nitric oxide synthase oxygenase dimer with active and inactive pterins. *Biochemistry* **2000**, *39*, 4608−4621.

(19) Kotsonis, P.; Frohlich, L. G.; Raman, C. S.; Li, H.; Berg, M.; et al. Structural basis for pterin antagonism in nitric-oxide synthase. Development of novel 4-oxo-pteridine antagonists of (6R)-5,6,7,8-tetrahydrobiopterin. *J. Biol. Chem.* **2001**, *276*, 49133−49141.

(20) Kotsonis, P.; Frohlich, L. G.; Shutenko, Z. V.; Horejsi, R.; Pfleiderer, W.; et al. Allosteric regulation of neuronal nitric oxide synthase by tetrahydrobiopterin and suppression of auto-damaging superoxide. *Biochem. J.* **2000**, *346* (Part 3), 767−776.

(21) Brandacher, G.; Zou, Y.; Obrist, P.; Steurer, W.; Werner-Felmayer, G.; et al. The 4-amino analogue of tetrahydrobiopterin efficiently prolongs murine cardiac-allograft survival. *J. Heart Lung Transplant* **2001**, *20*, 747−749.

(22) Bahrami, S.; Fitzal, F.; Peichl, G.; Gasser, H.; Fuerst, W.; et al. Protection against endotoxemia in rats by a novel tetrahydrobiopterin analogue. *Shock* **2000**, *13*, 386−391.

(23) Matter, H.; Kotsonis, P.; Klingler, O.; Strobel, H.; Frohlich, L. G.; et al. Structural requirements for inhibition of the neuronal nitric oxide synthase (NOS-I): 3D-QSAR analysis of 4-oxo- and 4-amino-pteridine-based inhibitors. *J. Med. Chem.* **2002**, *45*, 2923−2941.

(24) Kastenholz, M. A.; Pastor, M.; Cruciani, G.; Haaksma, E. E.; Fox, T. GRID/CPCA: a new computational tool to design selective ligands. *J. Med. Chem.* **2000**, *43*, 3033−3044.

(25) Goodford, P. J. A computational procedure for determining energetically favorable binding sites on biologically important macromolecules. *J. Med. Chem.* **1985**, *28*, 849−857.

(26) Boobbyer, D. N.; Goodford, P. J.; McWhinnie, P. M.; Wade, R. C. New hydrogen-bond potentials for use in determining energetically favorable binding sites on molecules of known structure. *J. Med. Chem.* **1989**, *32*, 1083−1094.

(27) Wade, R. C.; Clark, K. J.; Goodford, P. J. Further development of hydrogen bond functions for use in determining energetically favorable binding sites on molecules of known structure. 1. Ligand probe groups with the ability to form two hydrogen bonds. *J. Med. Chem.* **1993**, *36*, 140−147.

(28) Wade, R. C.; Goodford, P. J. Further development of hydrogen bond functions for use in determining energetically favorable binding sites on molecules of known structure. 2. Ligand probe groups with the ability to form more than two hydrogen bonds. *J. Med. Chem.* **1993**, *36*, 148−156.

(29) *GRID, V.* Molecular Discovery Ltd.: Oxford, U.K. **2001**.

(30) Westerhuis, J. A.; Kourti, T.; Macgregor, J. F. Analysis of multiblock and hierarchical PCA and PLS models. *J. Chemom.* **1998**, *12*, 301−321.

(31) Matter, H.; Defossa, E.; Heinelt, U.; Naumann, T.; Schreuder, H.; et al. Rational Approaches to Drug Design. *Proceedings of the 13th European Symposium on Quantitative Structure−Activity Relationships*; Prous, Barcelona, 2001; pp 177−185.

(32) Ridderstrom, M.; Zamora, I.; Fjellstrom, O.; Andersson, T. B. Analysis of selective regions in the active sites of human cytochromes P450, 2C8, 2C9, 2C18, and 2C19 homology models using GRID/CPCA. *J. Med. Chem.* **2001**, *44*, 4072−4081.

(33) Naumann, T.; Matter, H. Structural classification of protein kinases using 3D molecular interaction field analysis of their ligand binding sites: target family landscapes. *J. Med. Chem.* **2002**, *45*, 2366−2378.

(34) Terp, G. E.; Cruciani, G.; Christensen, I. T.; Jorgensen, F. S. Structural differences of matrix metalloproteinases with potential implications for inhibitor selectivity examined by the GRID/CPCA approach. *J. Med. Chem.* **2002**, *45*, 2675−2684.

(35) Pantke, M. M.; Reif, A.; Valtschanoff, J. G.; Shutenko, Z.; Frey, A.; et al. Pterin interactions with distinct reductase activities of NO synthase. *Biochem. J.* **2001**, *356*, 43−51.

(36) Frohlich, L. G.; Kotsonis, P.; Traub, H.; Taghavi-Moghadam, S.; Al-Masoudi, N.; et al. Inhibition of neuronal nitric oxide synthase by 4-amino pteridine derivatives: structure−activity relationship of antagonists of (6R)-5,6,7,8-tetrahydrobiopterin cofactor. *J. Med. Chem.* **1999**, *42*, 4108−4121.

(37) Yan, X.; Hollis, T.; Svinth, M.; Day, P.; Monzingo, A. F.; et al. Structure-based identification of a ricin inhibitor. *J. Mol. Biol.* **1997**, *266*, 1043−1049.

(38) Birdsall, D. L.; Finer-Moore, J.; Stroud, R. M. Entropy in bi-substrate enzymes: proposed role of an alternate site in chaperoning substrate into, and products out of, thymidylate synthase. *J. Mol. Biol.* **1996**, *255*, 522−535.

(39) Blundell, T.; Carney, D.; Gardner, S.; Hayes, F.; Howlin, B.; et al. 18th Sir Hans Krebs lecture. Knowledge-based protein modelling and design. *Eur. J. Biochem.* **1988**, *172*, 513−520.

(40) Sutcliffe, M. J.; Haneef, I.; Carney, D.; Blundell, T. L. Knowledge based modelling of homologous proteins, Part I: Three-dimensional frameworks derived from the simultaneous superposition of multiple structures. *Protein Eng.* **1987**, *1*, 377−384.

(41) Sutcliffe, M. J.; Hayes, F. R.; Blundell, T. L. Knowledge based modelling of homologous proteins, Part II: Rules for the conformations of substituted sidechains. *Protein Eng.* **1987**, *1*, 385−392.

(42) McMartin, C.; Bohacek, R. S. QXP: powerful, rapid computer algorithms for structure-based drug design. *J. Comput.-Aided Mol. Des.* **1997**, *11*, 333−344.

(43) Connolly, M. L. Solvent-accessible surfaces of proteins and nucleic acids. *Science* **1983**, *221*, 709−713.

(44) Connolly, M. L. Analytical molecular surface calculation. *J. Appl. Crystallogr.* **1983**, *16*, 548−558.

(45) Heiden, W.; Goetze, T.; Brickmann, J. Fast Generation of Molecular Surfaces from 3D Data Fields with an Enhanced "Marching Cube" Algorithm. *J. Comput. Chem.* **1993**, *14*, 246−250.

(46) Brickmann, J.; Bertling, H.; Bussian, B. M.; Knoblauch, M.; Waldherr-Teschner, M.; et al. *MOLCAD − Interaktive Molekulare Computergrafik auf High-Performance-Computern*; GDCh-Fachgruppe Chemie-Information: Würzburg, Tagungsbericht, 1987; pp 93−111.

(47) Nakane, M.; Pollock, J. S.; Klinghofer, V.; Basha, F.; Marsden, P. A.; et al. Functional expression of three isoforms of human nitric oxide synthase in baculovirus-infected insect cells. *Biochem. Biophys. Res. Commun.* **1995**, *206*, 511−517.

(48) Kuin, A.; Aalders, M.; van der Valk, M. A.; Frey, A.; Schmidt, H. H.; et al. Renal toxicity of the neuron-blocking and mitochondriotropic agent *m*-iodobenzylguanidine. *Cancer Chemother. Pharmacol.* **1998**, *42*, 37−45.

(49) Ghosh, D. K.; Wu, C.; Pitters, E.; Moloney, M.; Werner, E. R.; et al. Characterization of the inducible nitric oxide synthase oxygenase domain identifies a 49 amino acid segment required for subunit dimerization and tetrahydrobiopterin interaction. *Biochemistry* **1997**, *36*, 10609−10619.

(50) Ghosh, D. K.; Rashid, M. B.; Crane, B.; Taskar, V.; Mast, M.; et al. Characterization of key residues in the subdomain encoded by exons 8 and 9 of human inducible nitric oxide synthase: a critical role for Asp-280 in substrate binding and subunit interactions. *Proc. Natl. Acad. Sci. U.S.A.* **2001**, *98*, 10392−10397.

(51) Kabsch, W. Automatic processing of rotation diffraction data from crystals of initially unknown symmetry and cell constants. *J. Appl. Crystallogr.* **1993**, *26*, 795−800.

(52) Brunger, A. T.; Adams, P. D.; Clore, G. M.; DeLano, W. L.; Gros, P.; et al. Crystallography & NMR system: A new software suite for macromolecular structure determination. *Acta Crystallogr. D: Biol. Crystallogr.* **1998**, *54*, 905−921.

(53) Weiner, S. J.; Kollman, P. A.; Case, D. A.; Singh, U. C.; Ghio, C.; et al. A new force field for molecular mechanical simulation of nucleic acids and proteins. *J. Am. Chem. Soc* **1984**, *106*, 765−784.

(54) Viale die Casta. 16, *GOLPE Multivariate Infometric Analysis*; S.r.l.: Perugia, Italy, 1999.

(55) Baroni, M.; Costantino, G.; Cruciani, G.; Riganelli, D.; Valigi, R.; et al. Generating Optimal Linear PLS Estimations (GOLPE): An Advanced Chemometric Tool for Handling 3D-QSAR Problems. *Quant. Struct.−Act. Relat.* **1993**, *12*, 9−20.